Magnetics Integrated Design for CNR Point-of-Load Converter

Zehui Li[1], Zhongqiu Zhang[1], Qishan Pan[1], and Haoyu Wang[1,2]
[1] *School of Information Science and Technology, ShanghaiTech University, Shanghai, China*
[2] *Shanghai Engineering Research Center of Energy Efficient and Custom AI IC, Shanghai, China*
wanghy@shanghaitech.edu.cn

2026 IEEE Applied Power Electronics Conference and Exposition (APEC) | 979-8-3315-7544-1/26/$31.00 ©2026 IEEE | DOI: 10.1109/APEC51134.2026.11516876

***Abstract*—In data center point-of-load applications, current ninefold rectifier (CNR) converter offers obvious advantages over conventional current doubler rectifier (CDR), including zero-voltage switching (ZVS) and enhanced output current capability. However, the CNR typically employs three discrete transformers, resulting in a bulky design that compromises power density. Given the demanding requirements of data centers — particularly large voltage conversion ratios and high output currents — efficient magnetic design is crucial for achieving both high efficiency and high power density. To address this challenge, this paper presents a magnetic integration scheme tailored for the CNR converter, which substantially reduces transformer core volume. A 24 V-to-0.8 V, 180 A, 500 kHz CNR prototype incorporating the integrated magnetics is designed and experimentally validated. The prototype demonstrates a peak efficiency of 93.7% and maintains 89.6% efficiency at full load.**

***Index Terms*—Current doubler rectifier (CDR), current ninefold rectifier (CNR), data center, magnetic integration, voltage regulator (VR), zero-voltage switching (ZVS).**

I. Introduction

With the rapid advancement of modern information technologies, data center power consumption is surging and is projected to reach 8% of global electricity use by 2030 [1]. Consequently, the efficiency of power supplies has become increasingly critical. Raising the bus voltage reduces distribution losses, thereby improving overall system efficiency [2], [3]. However, achieving high efficiency under a large step-down ratio remains a major challenge for Point-of-Load (PoL) converters [4], [5]. Meanwhile, high-performance microprocessors demand currents exceeding 220 A at sub-1 V levels, and the wide input range from backup batteries imposes stringent regulation requirements [6]. In addition, the limited motherboard footprint necessitates ultra-high power-density solutions [7].

Multiphase Buck converter is a common solution for PoL converters in data centers [8]. However, when the bus voltage increases, Buck converter must operate with extremely small duty cycles, which not only imposes stricter requirements on the driver ICs but also hinders the achievement of high efficiency. The half-bridge current-doubler rectifier (CDR) is a derivative topology of the Buck converter [7], [9]. Compared with the Buck converter, the CDR introduces a transformer that enables a larger step-down ratio, making it a highly suitable solution for higher bus voltages. Nevertheless, the conventional half-bridge CDR suffers from hard switching of the primary-side devices, leading to significant voltage spikes and switching losses [9]. The current ninefold rectifier (CNR) — derived from the CDR — employs complementary pulse-width modulation (PWM) control to achieve zero-voltage switching (ZVS) for all primary-side switches. A nine-phase structure on the secondary side enhances power delivery. However, the three-phase transformer in CNR is bulky and limits the power density.

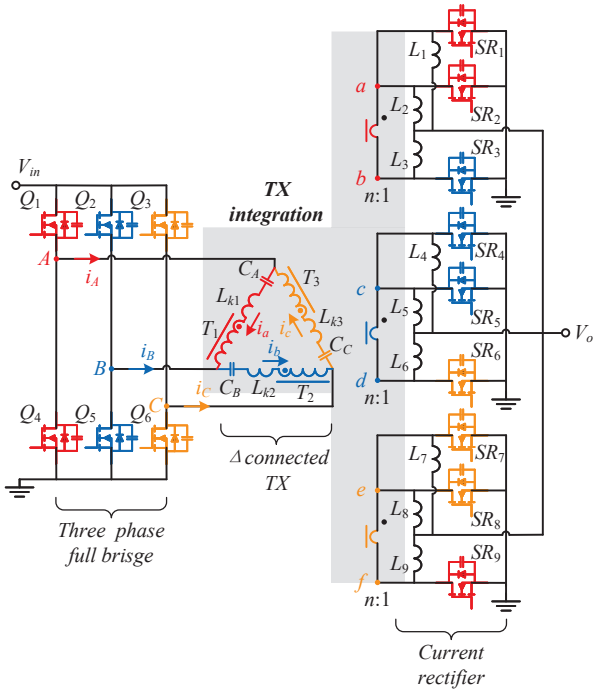

Fig. 1. Schematic of CNR topology with magnetic integration.

Magnetic components typically occupy the largest volume in power converters. Thus, optimizing magnetic design or employing magnetic integration can effectively enhance power density [7], [10]–[12]. In CDRs, the output inductors can be integrated into the transformer by utilizing the magnetizing inductor to improve the power density. For example, in [7] and [10], the transformer and output inductor are integrated into a single magnetic core, achieving higher power density. Moreover, a coupled-transformer structure is presented in [13], where the magnetizing inductor serves as the output inductor. These inductors are indirectly coupled through the transformer structure, enabling scalability and multiphase op-

This work was partially supported by the Natural Science Foundation of Shanghai under Grant 25ZR1401255.

Authorized licensed use limited to: ShanghaiTech University. Downloaded on June 25,2026 at 12:42:39 UTC from IEEE Xplore. Restrictions apply.

eration. Nevertheless, utilizing the transformer's magnetizing inductor as the output inductor reduces winding utilization and increases conduction loss [14]. This limitation hinders efficiency improvement, particularly in applications with large output currents. In [15], a coupled inductor integrates the discrete external inductors of parallel CDR modules to automatically balance the primary currents. However, this approach does not effectively reduce the magnetic component volume. A full-bridge half-turn transformer-based CDR is studied in [14]. It retains discrete output inductors and achieves good efficiency. However, this magnetic integration scheme is not suitable for CNR. To implement a half-turn transformer, the secondary modules must deliver two separate but ideally identical currents that form a single loop — one current path acting as the return for the other. Achieving this balance is difficult in CNR. To boost power density without compromising winding utilization, this paper proposes a magnetic integration scheme for the three-phase transformer. It preserves the key advantages of the CNR primary-side devices: achieving ZVS and maintaining low current stress.

The rest of this paper is organized as follows. Section II presents the operating principle of the CNR and the magnetic integration concept for the three-phase transformer. It derives the equivalent circuit of the integrated transformer and analyzes post-integration coupling issues. Section III details the design of the integrated planar transformer. Section IV shows experimental results from a CNR prototype rated at 24 V–0.8 V/180 A/500 kHz. Section V concludes the paper.

II. CNR Topology and Transformer Integration

A. CNR Topology

Fig. 1 shows the topology of the CNR and the concept of transformer integration. On the primary side, the topology employs a three-phase full-bridge combined with a Δ-connected transformer. The upper and lower switches in each bridge operate complementarily, with a 120° phase shift between adjacent phases. On the secondary side, the rectifier structure enhances output current capability, providing a scalable solution tailored to data center requirements.

Compared with the conventional half-bridge CDR topology, the CNR achieves ZVS for all primary-side switches, thereby reducing switching losses and suppressing voltage spikes. Compared with the PSFB CDR, the CNR benefits from current cancellation among primary windings enabled by the Δ configuration. This mechanism effectively reduces current stress on primary-side switches and improves efficiency under heavy-load conditions. Notably, the CNR adopts PWM control, a well-established technique that simplifies system modeling and control design.

B. Transformer Integration

The original CNR employs three discrete transformers, which occupy a considerable footprint. Minimizing transformer volume is essential for enhancing the power density of the CNR converter. According to the operating principle of the topology, the sum of the primary voltages of the three transformers is zero under steady-state conditions, as shown in Fig. 2.

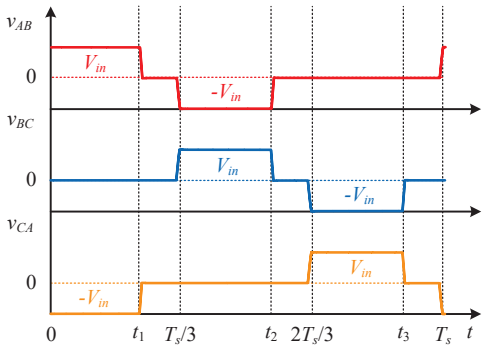

Fig. 2. Primary voltage waveforms of the CNR transformer within one switching cycle

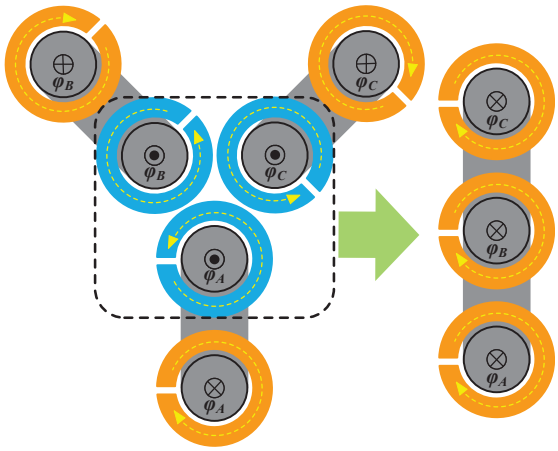

Fig. 3. Conceptual diagram of three U cores integrated into a single E core.

Based on Faraday's law, the primary winding voltage is:

$$v_{AB} = N \times (\frac{d\varphi_A}{dt}),\ v_{BC} = N \times (\frac{d\varphi_B}{dt}),\ v_{CA} = N \times (\frac{d\varphi_C}{dt}), \tag{1}$$

where, N is the number of turns of the primary windings. Since the sum of the primary voltages is zero, we have:

$$\frac{d\varphi_A}{dt} + \frac{d\varphi_B}{dt} + \frac{d\varphi_C}{dt} = 0, \tag{2}$$

which means that the net AC flux is canceled, allowing the magnetic structure to be represented by a single three-leg core, as illustrated in Fig. 3. Similarly, three EE cores can also be integrated into a single magnetic core, as shown in Fig. 4.

The equivalent circuit of the integrated transformer is shown in Fig. 5, where R_L denotes the reluctance of each magnetic leg and R_c represents the leakage reluctance [16]. Fig. 5 can be used to analyze the coupling issues arising from transformer integration. Since the three-phase full bridge operates in the same manner with only a 120° phase shift, the analysis is exemplified over one-third of the switching period (0–$T_s/3$).

As shown in Fig. 2, during 0–t_1, the primary switches Q_1, Q_5 and Q_6 are on, while Q_2, Q_3, and Q_4 are off, resulting in

Authorized licensed use limited to: ShanghaiTech University. Downloaded on June 25,2026 at 12:42:39 UTC from IEEE Xplore. Restrictions apply.

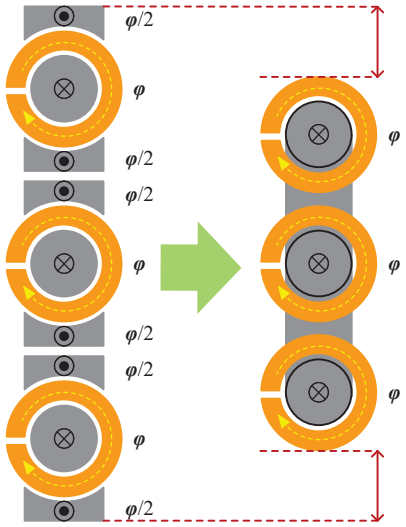

Fig. 4. Conceptual diagram of three E cores integrated into a single E core.

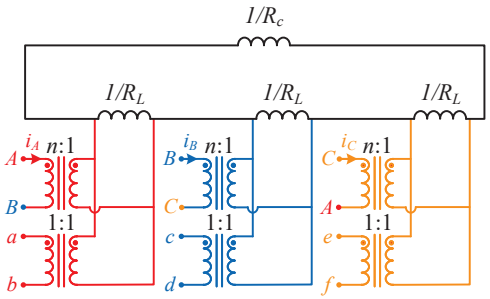

Fig. 5. Equivalent circuit diagram of the integrated three-phase transformer.

$v_{AB} = V_{in}$, $v_{BC} = 0$, and $v_{CA} = -V_{in}$. According to Fig. 5, the voltage across $1/R_c$ is $V_{in}/n + 0/n + (-V_{in})/n$, which equals to 0.

During t_1–$T_s/3$, all upper switches (Q_1–Q_3) are off, and all lower switches (Q_4–Q_6) are on, yielding $v_{AB} = v_{BC} = v_{CA} = 0$. Consequently, the voltage across $1/R_c$ remains zero, and its current is constant throughout t_0–$T_s/3$. Similarly, during $T_s/3$–T_s, the voltage across $1/R_c$ is always zero, indicating that the integrated transformer does not generate any coupling current.

III. Design of Planar Transformer

The design of the planar transformer mainly involves the determination of the turns ratio, the selection of core material, and the optimization of core dimensions. The transformer turns ratio is closely related to the voltage gain requirements of the topology. The voltage gain of the CNR is given in (3):

$$\frac{V_o}{V_{in}} = \frac{D}{n}, \tag{3}$$

where n is the turns ratio of the transformer, and D is the duty cycle of the primary-side upper switches. According to (3), in order to achieve a voltage conversion from 24 V to 0.8 V

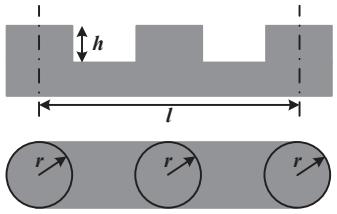

Fig. 6. Dimensions of the designed magnetic core.

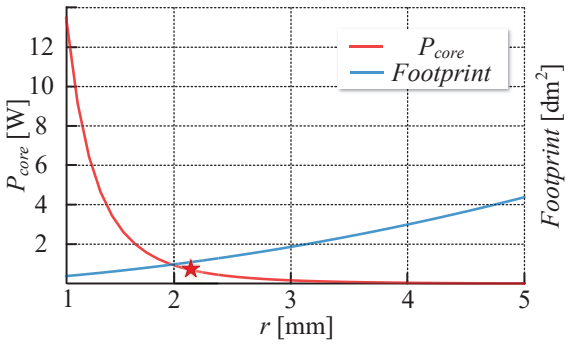

Fig. 7. Magnetic core dimensions optimization based on the trade-off between core loss and footprint.

while ensuring that D does not exceed $1/3$, the transformer turns ratio n must satisfy the following inequality:

$$n < \left[\frac{V_{in}}{3V_o}\right]_{\min} = \frac{24}{3 \times 0.8} = 10. \tag{4}$$

For the CNR topology, a higher transformer turns ratio n can effectively reduce the current stress on the primary-side switches and decrease the conduction losses. Moreover, increasing the number of primary winding turns enhances the primary-side leakage inductance, which helps extend the ZVS operating range of the primary switches. Therefore, a turns ratio of $n = 8$ is selected in this design. To achieve an 8:1 turns ratio, the primary winding is implemented with eight turns connected in series on each magnetic core, while the secondary windings are configured with eight turns in parallel.

The dimension optimization of the transformer is crucial for achieving high efficiency and high power density in CNR. The main target is balancing the transformer's loss and footprint. The size is parameterized in Fig. 6. Thus, the total footprint of the transformer is

$$V_{core} = 6 \times \pi r^2 \times h + 2 \times [2r \times l \times \frac{\pi r^2}{2r} + \pi r^2 \times \frac{\pi r^2}{2r}]. \tag{5}$$

The effective core cross-sectional area A_e is selected based on magnetic loss constraints, as indicated in (6):

$$\Delta B \geq \frac{V_{in} D}{2 n f_s A_e} = \frac{V_{in} D}{2 n f_s \pi r^2}, \tag{6}$$

where, ΔB is the maximum acceptable magnitude of magnetic flux. A_e should satisfy this constraint to limit the core loss.

The core loss and winding loss of the transformer can be evaluated by the Steinmetz equation and Dowell's model,

Authorized licensed use limited to: ShanghaiTech University. Downloaded on June 25,2026 at 12:42:39 UTC from IEEE Xplore. Restrictions apply.

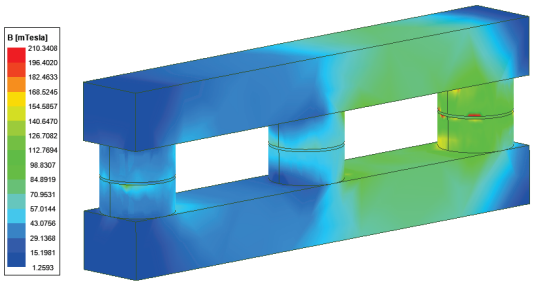

Fig. 8. Finite-element simulation results of the designed magnetic core in ANSYS MAXWELL.

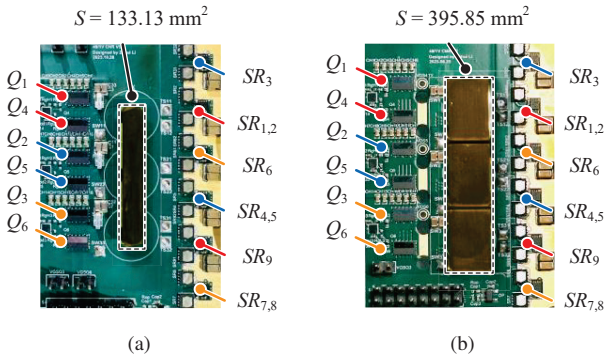

Fig. 9. Photograph of the experimental prototypes: (a) CNR prototype with integrated three-phase transformer, and (b) CNR prototype with discrete transformers.

respectively [11]. Considering the relationship between core loss and dimensions, as well as footprint constraints, the transformer dimensions can be optimized, as illustrated in Fig. 7. Since h is determined by the PCB thickness and l can be determined by the winding width and the magnetic core radius r, the core volume can be regarded as a function of r, according to (5). As shown in Fig. 7, increasing the radius r reduces the core loss but simultaneously enlarges the footprint. To achieve a trade-off between core loss and footprint, the magnetic leg radius is selected as $r = 2.2\ mm$ in the optimized design. The DMR51W core material from DMEGC is selected to achieve high-frequency optimization. The flux density distribution of the designed core, simulated in ANSYS MAXWELL, is shown in Fig. 8. It is worth noting that, to obtain relatively accurate magnetic simulation results, the equivalent circuit shown in Fig. 5 is modeled in MATLAB/SIMULINK. The simulated transformer currents are then used as excitation inputs. Finite-element analysis indicates that the magnetic flux in the designed core is uniformly distributed.

IV. Experimental Results

To validate the concept, a 24 V/0.8 V/180 A CNR prototype with integrated transformer is designed, as shown in Fig. 9 (a). As shown in Fig. 9 (a), the footprint of the integrated transformer is approximately 133.13 mm^2. In comparison, the footprint of the discrete three-phase transformer in the CNR

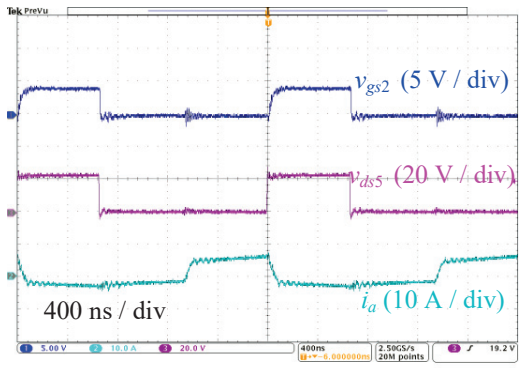

Fig. 10. Experimental waveforms for 24 V/0.8 V/180 A operation.

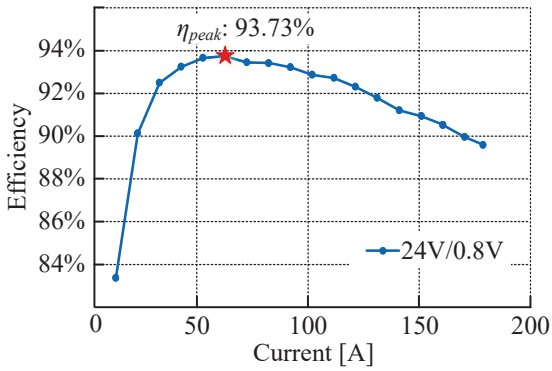

Fig. 11. Efficiency curve versus load current at an output voltage of 0.8 V with an input voltage of 24 V.

TABLE I
Specifications of the Prototype

Parameter	Specification
Primary switches	EPC2306
Synchronous rectifiers	IQE004NE1LM7CGSC IQE004NE1LM7SC
Magnetic core	DMR51W ECW14.5A (DMEGC)
Switching frequency f_s	500 kHz
Input voltage V_{in}	24 V
Output voltage V_o	0.8 V
Output current I_o	180 A
Transformer turns ratio n	8:1
Output inductance L_o	300 nH

prototype, shown in Fig. 9 (b), is about 395.85 mm^2. Therefore, transformer integration effectively reduces the footprint by approximately 2/3.

The specifications of the prototype are summarized in Table I. The electronic load is Chroma 63206A, the DC source is Chroma 62100H, and the controller is a TI TMS320F280039C.

Experimental waveforms for 24 V/0.8 V/180 A operation are shown in Fig. 10. The phase-shifted gate signals of Q_1,

Authorized licensed use limited to: ShanghaiTech University. Downloaded on June 25,2026 at 12:42:39 UTC from IEEE Xplore. Restrictions apply.

Fig. 12. Thermal image of the prototype under full-load operation.

Q_2 and Q_3 exhibit identical switching patterns with 120° separation. Taking Q_2 as an example, Fig. 10 illustrates v_{gs2}, v_{ds5}, and the primary transformer current i_a. Q_2 and Q_5 operate in a complementary manner, enabling ZVS turn-on through the dead time. When Q_2 is on and Q_5 is off, v_{AB} equals $-V_{in}$. At this instant, the primary current of transformer T_1 is equal to $1/n$ of the magnetizing current of L_3. Because this current flows out of the same-named terminal of the primary winding, it is observed as a negative current.

Fig. 11 shows the efficiency curve versus load current at an output voltage of 0.8 V with an input voltage of 24 V. The peak efficiency reaches 93.73% at 60 A. Meanwhile, the CNR topology maintains high efficiency under heavy-load conditions, with a full-load efficiency of 89.61% at 180 A. It is worth noting that the magnetic integration of the three-phase transformer does not affect the operating principle of the CNR. This integration reduces the transformer volume while preserving the advantages at the primary side, achieving ZVS and maintaining low current stress.

The thermal image of the prototype under full-load operation is captured in Fig. 12. As observed, at a load current of 180 A, the temperature distribution is relatively uniform, with the major losses concentrated in the secondary synchronous rectifiers and windings. The relatively low temperature of the magnetic core under full-load operation demonstrates that the magnetic design effectively controls core losses.

V. Conclusions

This work proposes a magnetic integration scheme for CNR converter. The equivalent circuit of the integrated three-phase transformer is analyzed, coupling issues are discussed, and a detailed transformer design process is provided. A 24 V-0.8 V/500 kHz/180 A prototype is built and experimentally validated. The results demonstrate a peak efficiency of 93.73% at 60 A and a full-load efficiency of 89.61% at 180 A. The integrated design reduces transformer volume while preserving the advantages of the primary-side devices, including ZVS operation and low current stress. The proposed three-phase integrated transformer effectively decreases the magnetic component volume of the CNR, thereby satisfying the demanding requirements of high step-down ratio, high output current, high efficiency and high power density in modern data center voltage regulators.

Acknowledgment

The authors would like to thank Hengdian Group DMEGC Magnetics for customizing the ferrite core samples for this research.

References

[1] S. Clement, K. Burdett, N. Rteil, A. Wynne, and R. Kenny, "Is Hot IT a False Economy? An Analysis of Server and Data Center Energy Efficiency as Temperatures Rise," *IEEE Trans. on Sustainable Comput.*, vol. 9, no. 3, pp. 482–493, May–June 2024.

[2] Y. Chen, K. Shi, M. Chen, and D. Xu, "Data center power supply systems: From grid edge to point-of-load," *IEEE J. Emerg. Sel. Top. Power Electron.*, vol. 11, no. 3, pp. 2441–2456, Jun. 2023.

[3] L. Wang, C. Li, J. Liang, W. T. Ng, and H. Wang, "Analysis and design of ultrafast series capacitor trans-inductor voltage regulator with constant on-time control," *IEEE Trans. Power Electron.*, vol. 40, no. 6, pp. 8315–8327, Jun. 2025.

[4] M. H. Ahmed, C. Fei, F. C. Lee, and Q. Li, "Single-Stage High-Efficiency 48/1V Sigma Converter With Integrated Magnetics," *IEEE Trans. Ind. Electron.*, vol. 67, no. 1, pp. 192–202, Jan. 2020.

[5] J. Liang, L. Wang, C. Li, J. Liang, M. Fu, and H. Wang, "Topology and magnetics integrated design for switched-capacitor llchybrid 48 v–1 v dcx in data center applications," *IEEE Trans. Power Electron.*, vol. 41, no. 1, pp. 781–790, Jan. 2026.

[6] J. Liang, Y. Qin, Y. Liu, M. Fu, and H. Wang, "Phase Shift Regulated Resonant Switched-Capacitor-Based Intermediate Bus Converter for 48 V Data Center Power System," *IEEE Trans. Ind. Electron.*, vol. 72, no. 2, pp. 1475–1485, 2025.

[7] X. Lou and Q. Li, "Single-Stage 48V/1.8V Converter With a Novel Integrated Magnetics and 1000 W/in^3 Power Density," *IEEE Trans. Ind. Electron.*, vol. 71, no. 7, pp. 6601–6611, Jul 2024.

[8] C. Fei, M. H. Ahmed, F. C. Lee, and Q. Li, "Two-Stage 48 V-12 V/6 V-1.8 V Voltage Regulator Module With Dynamic Bus Voltage Control for Light-Load Efficiency Improvement," *IEEE Trans. Power Electron.*, vol. 32, no. 7, pp. 5628–5636, Jul. 2017.

[9] Z. Li, Q. Pan, J. Liang, J. Liang, M. Fu, and H. Wang, "Active Clamped Half-Bridge CDR Converter for 48 V Data Center Voltage Regulator Modules," *IEEE Trans. Ind. Electron.*, pp. 1–10, 2025.

[10] F. Li, L. Wang, and L. Yu, "A Novel Integrated Matrix Magnetics for Isolated Single-Stage DC–DC Converter," *IEEE Trans. Power Electron.*, vol. 37, no. 10, pp. 12 380–12 390, Oct 2022.

[11] C. Fei, F. C. Lee, and Q. Li, "High-Efficiency High-Power-Density LLC Converter with an Integrated Planar Matrix Transformer for High-Output Current Applications," *IEEE Trans. Ind. Electron.*, vol. 64, no. 11, pp. 9072–9082, Nov 2017.

[12] M. Fu, C. Fei, Y. Yang, Q. Li, and F. C. Lee, "Optimal Design of Planar Magnetic Components for a Two-Stage GaN-Based DC–DC Converter," *IEEE Trans. Power Electron.*, vol. 34, no. 4, pp. 3329–3338, Apr. 2019.

[13] X. Lou, F. Zhu, Z. Li, Q. Li, and F. C. Lee, "Single-stage 48 v/1.8 v coupled-transformer voltage regulator (ctvr)," in *IEEE Energy Convers. Congr. Expo. (ECCE)*. Nashville, TN, USA: IEEE, Oct. 2023, pp. 2333–2339.

[14] X. Xu and Q. Li, "Single-stage 48v-to-1v regulator with a half-turn transformer and current-doubler rectifier," in *IEEE Appl. Power Electron. Conf. Expo. (APEC)*, Mar. 2025, pp. 1433–1438.

[15] F. Li, L. Wang, M. Wu, and L. Yu, "A coupled-inductor-based input-parallel output-parallel quasi-resonant single-stage dc–dc converter to mitigate current difference," *IEEE Trans. Ind. Electron.*, vol. 71, no. 7, pp. 6512–6523, Jul. 2024.

[16] P. Wang, D. H. Zhou, Y. Elasser, J. Baek, and M. Chen, "Matrix coupled all-in-one magnetics for pwm power conversion," *IEEE Trans. Power Electron.*, vol. 37, no. 12, pp. 15 035–15 050, Dec. 2022.

Authorized licensed use limited to: ShanghaiTech University. Downloaded on June 25,2026 at 12:42:39 UTC from IEEE Xplore. Restrictions apply.